Chemical Engineering Journal 242 (2014) 76–85

Contents lists available at ScienceDirect

Chemical Engineering Journal

journal homepage: www.elsevier.com/locate/cej

Support modification for improving the performance of MnO_x–CeO_y/γ-Al_2O_3 in selective catalytic reduction of NO by NH_3

Long Qu [a,b], Caiting Li [a,b,*], Guangming Zeng [a,b], Mengying Zhang [a,b], Mengfan Fu [a,b], Jinfeng Ma [a,b], Fuman Zhan [a,b], Diqiang Luo [a,b]

[a] College of Environmental Science and Engineering, Hunan University, Changsha 410082, PR China
[b] Key Laboratory of Environmental Biology and Pollution Control, Hunan University, Ministry of Education, Changsha 410082, PR China

HIGHLIGHTS

- Zr, Ti and Si were used to combine with Al as supports for Mn–Ce SCR catalysts.
- The SCR activity of MCA was enhanced by support modification.
- The deactivating effects of SO_2 on SCR could be reduced by addition of ZrO_2.
- The promotion brought by ZrO_2 addition was investigated comprehensively.

ARTICLE INFO

Article history:
Received 16 October 2013
Received in revised form 21 December 2013
Accepted 23 December 2013
Available online 3 January 2014

Keywords:
NO
γ-Al_2O_3
ZrO_2
Catalytic activity
Environment

ABSTRACT

The catalytic performances of catalysts with binary-oxides supports in selective catalytic reduction (SCR) of NO by NH_3 were studied. Binary metal oxides supports γ-Al_2O_3–SiO_2, γ-Al_2O_3–TiO_2, and γ-Al_2O_3–ZrO_2 were prepared by hydrolyzation and coprecipitation methods, after that MnO_x–CeO_y was loaded using isovolumetric impregnation method. Characterizations for the samples involved N_2 adsorption–desorption, X-ray diffraction (XRD), X-ray photoelectron spectroscopy (XPS), H_2 temperature programmed reduction (H_2-TPR) and Fourier Transform infrared spectroscopy (FTIR). In the SCR tests, MnO_x–CeO_y/γ-Al_2O_3–ZrO_2 (MCAZ) showed outstanding NO removal efficiency and could abate the deactivation brought by SO_2 and H_2O. Moreover, the fluctuation of gas hourly space velocity (GHSV) appeared only a bit of influence on the activity at middle temperature. The characterization results exhibited that MnO_x–CeO_y/γ-Al_2O_3–ZrO_2 owned bigger specific surface area and appropriate pore diameter, highly dispersed amorphous Mn_2O_3 as well as rational ratio of Ce^{4+}/Ce^{3+}. The H_2-TPR results presented the promotion of the activity was partially due to the stronger oxidation ability at low temperature. Through the FTIR analysis, and combining with the mechanism proposed by earlier research, it was supposed that the highly reactive nitrates on the surface favored the high NO conversion. Besides, FTIR revealed that the bidentate sulfates formed by adsorbed SO_2 produced new Lewis acid sites which promoted NH_3 adsorption and reduced the poisoning effect of SO_2 and H_2O.

1. Introduction

Nitrogen oxides (NO, NO_2, and N_2O) emitted by stationary sources and mobile sources were the major sources of air pollution [1–3]. Due to the outstanding removal efficiency, highly N_2 selectivity and reasonable economic costs, selective catalytic reduction (SCR) is regarded as one of the most effective post-combustion technologies for the abatement of nitrogen oxides emission [1,4,5]. However, as the most widely engaged catalysts, V_2O_5/TiO_2 (with addition of WO_3 or MoO_3) catalysts are efficient only within a narrow temperature window of 300–400 °C, that means the SCR reactor has to be installed upstream the particulate collector and desulfurization, under which circumstance the catalyst will be attritted, sintered and poisoned by the dust and SO_2 in the flue gas soon [6–8]. Furthermore, the H_2O in the flue gas contributes to partially destroying the acid sites and then leads to the catalyst's deactivation [9,10]. Considering these handicaps, placing the reactor downstream the particulate collector and desulfurization is a feasible solution. Therefore, the catalysts with excellent activity at low temperature and stable resistance to both SO_2 and H_2O receive quantities of attention in recent years.

To improve the catalyst's performance, innovation of synthetic methods and component modification are considered as two crucial ways that work well. Thirupathi Boningari et al. optimized

* Corresponding author at: College of Environmental Science and Engineering, Hunan University, Changsha 410082, PR China. Tel./fax: +86 731 88649216.
E-mail addresses: ctli@hnu.edu.cn, ctli3@yahoo.com (C. Li).

1385-8947/$ - see front matter © 2013 Elsevier B.V. All rights reserved.
http://dx.doi.org/10.1016/j.cej.2013.12.076

commercial SCR catalysts by adopting flame spray pyrolysis (FSP) synthesis technique [11] and investigated vanadia-based nanoparticles prepared by FSP with various supports [12]. In another way, component modification is more generally investigated due to its diversity as well as pertinence. Manganese oxides have attracted much interest for its high activity in NH_3-SCR at low temperature. It has been corroborated that the activity of NO conversion is correlated with the valence of manganese and phase structure of MnO_x [6,13]. Ceria has also been extensively studied as a SCR catalyst owing to its oxygen storage and redox properties [14,15]. Accordingly, scholars have tried a variety of Mn–Ce catalysts with different supports, such as MnO_x–CeO_y binary-oxides catalyst [14,16–18], Mn–Ce/TiO_2 [19–21], Mn–Ce/Al_2O_3 [20] and Mn–Ce/ZSM5 [22]. However, due to the distinctive properties of different support materials, each of them exhibits some bottlenecks which limit its application and further research [6,23,24]. Always, the carrier in the catalyst plays a role which affects the surface properties [25,26], mechanical properties, thermal stability [27,28], sulfur resistance [26,29,30] and SCR catalytic performance [23,31,32] of the catalyst. The doping of other metal oxides in the support aims at overcoming the weaknesses of the existing supports. Catalysts with binary-oxides carrier such as Ce/TiO_2–SiO_2 [26], Ce/TiO_2–Al_2O_3 [26], Mn/γ-Al_2O_3(80%)–TiO_2(20%) [33], ZrO_2–V_2O_5/WO_3–TiO_2 [34] and MnO_x/$Ce_{0.5}Zr_{0.5}O_2$ [29] are investigated recently. After the addition into the supports, indispensable properties including stronger sulfur resistance, higher specific surface areas and considerable redox abilities were confirmed, according to their SCR performances and characterization results.

In this study, aiming at promoting the SCR activities and resistance to SO_2 and H_2O, a second metal oxide (SiO_2, TiO_2 or ZrO_2) was added into the support to modify MnO_x–CeO_y/γ-Al_2O_3. Besides, the superficial reaction stability and the effects of different gas hourly space velocities (GHSV) on the catalysts were also investigated respectively. To further investigate the changes of surface properties brought by the addition of the second metal, N_2 adsorption–desorption, X-ray diffraction (XRD), X-ray photoelectron spectroscopy analysis (XPS), H_2 temperature programmed reduction (H_2-TPR) and Fourier Transform infrared spectroscopy (FTIR) were carried out and analyzed in detail.

2. Experimental section

2.1. Preparation of catalysts

2.1.1. Preparation of MnO_x/γ-Al_2O_3, MnO_x–CeO_y/γ-Al_2O_3, MnO_x–CeO_y/TiO_2, MnO_x–CeO_y/SiO_2 and MnO_x–CeO_y/ZrO_2

In order to ascertain the best loading proportion of the active components (MnO_x and CeO_y), a series of MnO_x/γ-Al_2O_3 and MnO_x–CeO_y/γ-Al_2O_3 were prepared by isovolumetric impregnation method. A requisite amount of manganese acetate (or both manganese acetate and cerium nitrate) was dissolved in ultrapure water, and then the γ-Al_2O_3 powder was added into the solution and uniformly mixed, The mixtures were impregnated for 24 h, dried at 100 °C for 6 h and calcined in a muffle furnace at 500 °C for 4 h. MnO_x–CeO_y/TiO_2, MnO_x–CeO_y/SiO_2 and MnO_x–CeO_y/ZrO_2 were prepared by isovolumetric impregnation method using the best loading proportion of MnO_x and CeO_y.

2.1.2. Preparation of binary-oxides supports

In our work, γ-Al_2O_3–TiO_2 and γ-Al_2O_3–SiO_2 binary-oxides supports were prepared by hydrolyzation method while γ-Al_2O_3–ZrO_2 was prepared by coprecipitation method. The proportions of γ-Al_2O_3/M are 3:1, 1:1, 1:3 (M represents TiO_2, SiO_2 or ZrO_2, mole ratio) in the catalyst supports. A requisite amount of aluminum isopropoxide was dissolved in ultrapure water in the beakers. The solutions were continuously stirred and heated in a water bath at 40 °C, after that the oxalic acid ($H_2C_2O_4{\cdot}2H_2O$) solution and tetraethyl orthosilicate (TEOS), or oxalic acid and tetrabutyl titanate ($C_{16}H_{36}O_4Ti$) were slowly added into the above solution respectively under vigorously stirring in a water bath at 60 °C. The mixtures were filtered, washed several times, dried at 100 °C overnight, and then calcined in air at 500 °C for 4 h to produce γ-Al_2O_3–TiO_2 and γ-Al_2O_3–SiO_2. In the preparing process of γ-Al_2O_3–ZrO_2, both aluminum nitrate and zirconium nitrate were dissolved into ultrapure water in a water bath at 40 °C, and then excess diluted ammonia was slowly dropped to the mixture solution until pH 9 with vigorously stirring in a water bath at 60 °C. The mixtures were filtered, washed several times, dried at 100 °C overnight, then calcined in air at 500 °C for 4 h to produce γ-Al_2O_3–ZrO_2.

2.1.3. Preparation of loaded catalyst

Isovolumetric impregnation method was used to prepare loaded catalyst; the process was the same as Section 2.1.1.

Finally, MnO_x/γ-Al_2O_3, MnO_x–CeO_y/γ-Al_2O_3, MnO_x–CeO_y/SiO_2, MnO_x–CeO_y/TiO_2, MnO_x–CeO_y/ZrO_2, MnO_x–CeO_y/γ-Al_2O_3–SiO_2, MnO_x–CeO_y/γ-Al_2O_3–TiO_2, and MnO_x–CeO_y/γ-Al_2O_3–ZrO_2 catalysts were prepared and denoted as MA, MCA, MCS, MCT, MCZ, MCAS(a), MCAT(b) and MCAZ(c), respectively. The letters a, b and c represented the mole ratios of Al_2O_3 to SiO_2, TiO_2 and ZrO_2.

2.2. Apparatus and catalytic experiments

The SCR activity was tested in a fixed bed quartz reactor system. It consisted of a vertical quartz tube (20 mm nominal ID × 406.4 mm long) and a 3-zone temperature controlled furnace (Fig. 1). Fine catalyst powder was pressed into thin wafers, then crushed and sieved within a size range of 40–80 mesh. In each test, 500 mg catalyst was used while the temperature ranged from 60 °C to 380 °C. The reaction conditions were as follows: total flow rate was 350 mL/min, which corresponded to a GHSV of approximately 20,000 h^{-1}. Small variations (about 10%) existed due to the different densities of catalysts. Effects of the environmental conditions could be ignored because the tests were operated under the similar testing conditions (approximately 27.5 °C and 1007 hPa). The simulated flue gas was composed of 1000 ppm NO, 1000 ppm NH_3, 5% O_2, 500 ppm SO_2 (when used), 5% H_2O vapor (when used) and N_2 as the balance gas. A peristaltic pump transferred water into the stainless steel tube wrapped with a temperature-controlled heating tape and then H_2O (g) was generated. The heated N_2 took the H_2O (g) along and mixed with the flue gas. A set of mass flow controllers was used to control every kind of gas accurately. The gas compositions in the inlet and outlet were analyzed by a flue gas analyzer (Testo 350 XL, Germany).

The total conversion of NO was calculated from the equation below:

$$\text{NO Removal Efficiencey } (\%) = \frac{[NO]_{inlet} - [NO]_{outlet}}{[NO]_{inlet}} \times 100\%$$

where $[NO]_{inlet}$ is the inlet NO concentration (ppm) and $[NO]_{outlet}$ is outlet NO concentration (ppm).

2.3. Catalyst characterization

2.3.1. Specific surface area and pore diameter analysis

The specific surface areas of the catalysts were measured using a Micromeritics ASAP 2020 M+C volumetric sorption analyzer (Micromeritics Instrument Corp., USA) at 77 K. Each sample was degassed for 16 h at 250 °C before the isotherms were measured by standard nitrogen adsorption. The specific surface areas were

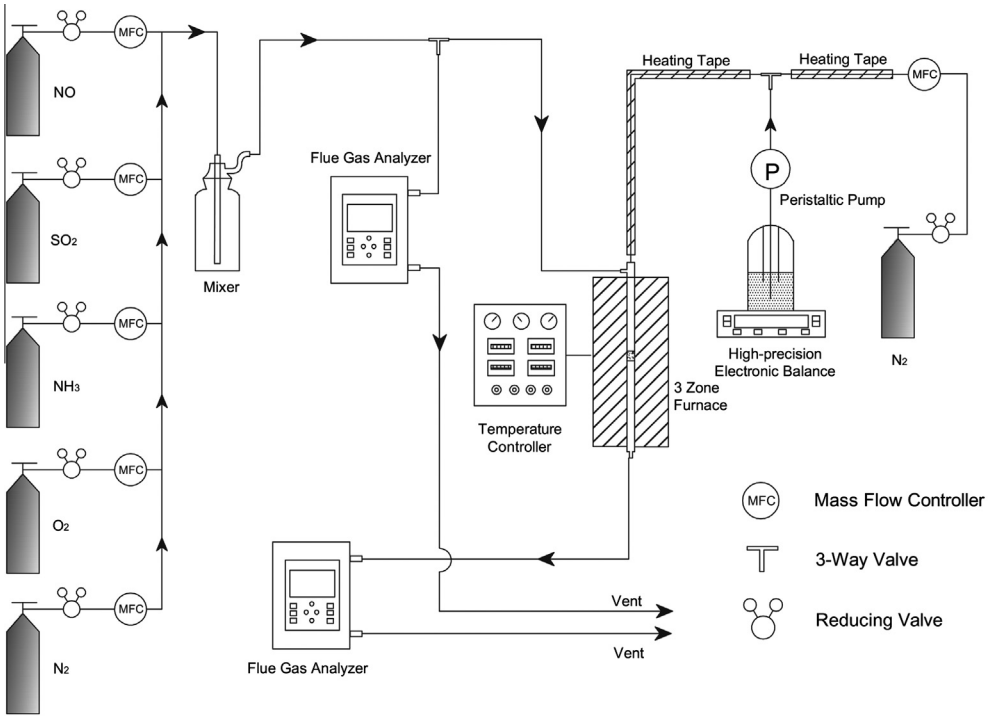

Fig. 1. Schematic diagram of the experimental setup.

calculated by the BET (Brunauer–Emmett–Teller) method, while the pore size distributions were obtained from the desorption branches of N_2 adsorption isotherm and calculated by the BJH (Barrett–Joyner–Halenda) formula.

2.3.2. X-ray diffraction (XRD)

To examine the crystallinity and dispersity of the species in the catalysts, X-ray powder diffraction patterns were carried out on a Bruker D8-Advance X-ray diffraction equipment, under the following conditions: Cu target Kα ray (λ = 0.1543 nm); scanning voltage 40 kV, scanning current 40 mA; scanning speed 0.2 s, scanning step 0.02°.

2.3.3. X-ray photoelectron spectroscopy (XPS)

The oxidation states of the metals on the surface of catalysts were analyzed by X-ray photoelectron spectroscopy performed on a K-Alpha 1063 X-ray photoelectron spectrometer (Thermo Fisher Scientific, USA) using 72 W Al Kα radiation from micro aggregation monochromator. The binding energies were referenced to the C 1s line at 284.6 eV from adventitious carbon.

2.3.4. H_2 temperature programmed reduction (H_2-TPR)

The H_2-TPR experiments were performed on a custom made thermal conductivity detector (TCD) setup using 50 mg catalysts. Prior to H_2-TPR experiments, catalysts were pretreated at 300 °C for 1 h in nitrogen (50 mL/min) and then the sample temperature was lowered to 100 °C. A feed containing 6 vol% H_2 in Ar was fed to the catalyst at a flow rate of 50 mL/min and the temperature of the catalyst was raised from 100 to 800 °C at a heating rate of 10 °C min^{-1}. The hydrogen consumption was measured quantitatively by a TCD.

2.3.5. Fourier transform infrared spectroscopy (FTIR)

FTIR spectroscopy studies were carried out with a SHIMADZU FTIR-8400S IRprestige-21 apparatus. Its resolution factor was 2 cm^{-1} from 400 cm^{-1} to 4000 cm^{-1} and scans were collected at a scan speed of 5 kHz. Circular self-supporting wafers of different samples were used. Powders of the samples (2 mg) were grinded and mixed with KBr (200 mg, spectroscopically pure) before tableting on a hydraulic press. The pretreatment process was as follows: samples were purged with high purity nitrogen for 2 h at 300 °C, after that several combinations of different gases were introduced to the reaction tube for 60 min at 50 °C. The gases combinations included $NH_3 + N_2$, $NO + O_2 + N_2$, $SO_2 + O_2 + N_2$ and $SO_2 + O_2 + H_2O + N_2$. The last step was N_2 purging at 200 °C for 30 min. The FTIR experiments were conducted immediately after the pretreatment.

3. Results and discussion

3.1. SCR catalytic activity

Initially, the potential catalytic performance of Mn/γ-Al_2O_3 and Mn–Ce /γ-Al_2O_3 were evaluated (using the feed: 1000 ppm NO, 1000 ppm NH_3, 5% O_2 and N_2 as the balance gas) to optimize the loading amount of Mn and Ce and to investigate the influence of Mn + Ce co-cations on NO removal efficiency. Afterward the optimal proportions of the metal oxides in the supports were investigated. All these results were supplied in the Supplementary data.

3.1.1. The activity of catalysts with single and binary-oxides supports

The SCR performances over catalysts with various supports operating under specified experimental condition were displayed in Fig. 2.

It could be seen from Fig. 2(a), with the same loading amount of Mn and Ce, MCA, MCT and MCZ displayed high SCR activities with a similar tendency. However, MCS was much inactive with its best removal efficiency of 75% at 340 °C. MCA performed the best removal efficiency almost in the whole temperature range and approximately 95% conversion was obtained at its highest efficiency temperature (250 °C). Different with MCT, MCZ was a little more active at middle temperature and less active at higher temperature. Fig. 2(b) illustrated that the NO removal efficiency increased rapidly over low temperature range after the addition.

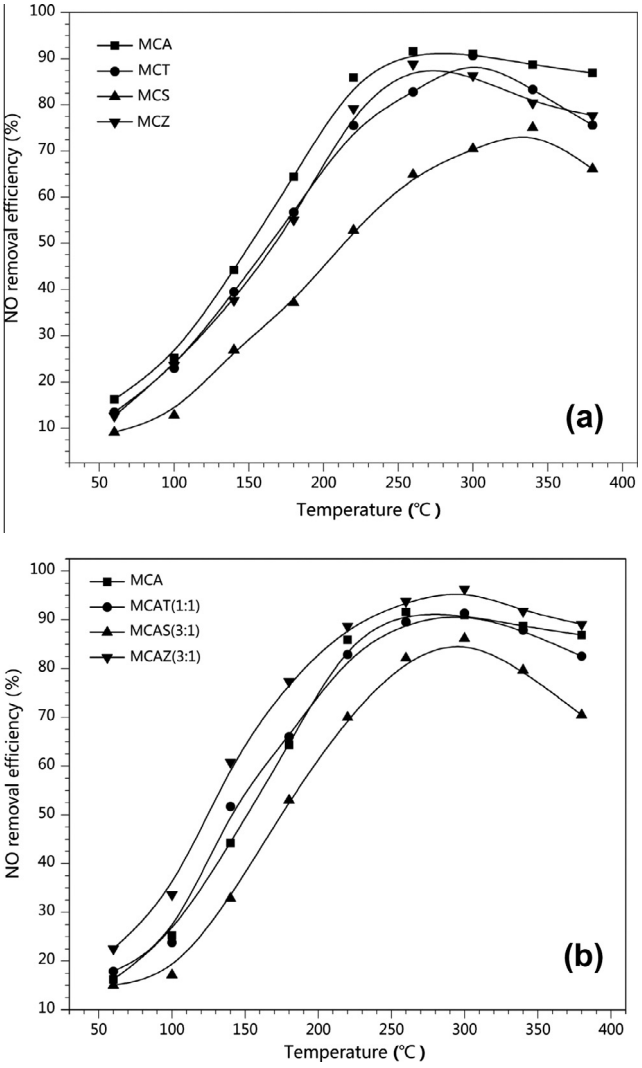

Fig. 2. NO removal efficiency during the SCR reaction over (a) single metal support catalysts and (b) binary-metals support catalysts. (Reaction condition: 1000 ppm NO, NH_3/NO: 1, 5% O_2, 500 mg of sample, 350 mL/min total flow rate and GHSV 20,000 h^{-1}.)

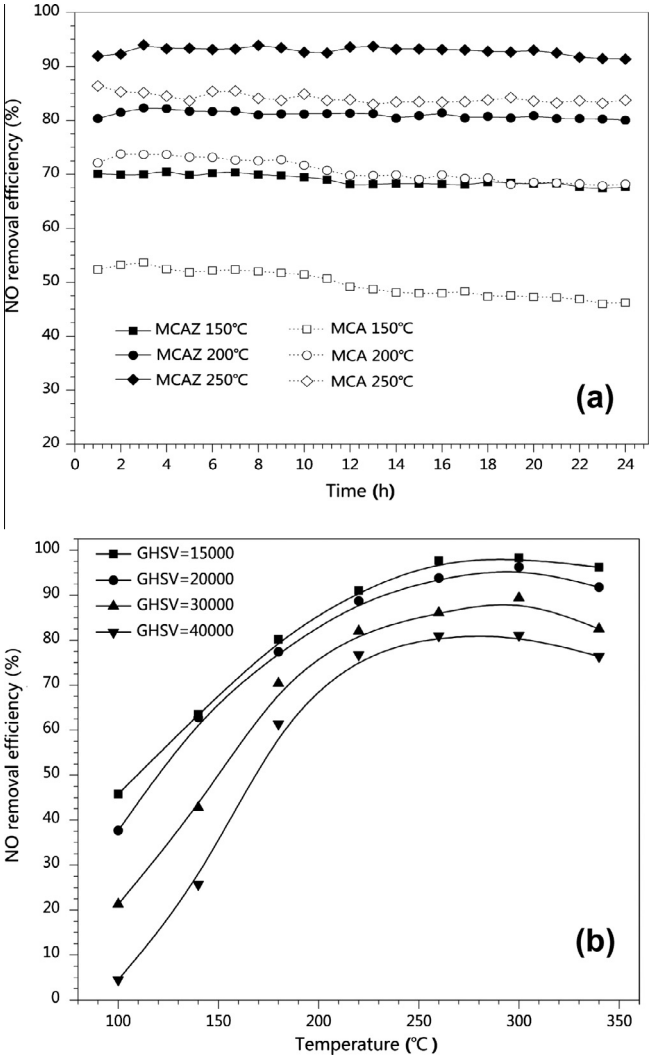

Fig. 3. (a)The catalytic stability of MCA and MCAZ at 150 °C, 200 °C and 250 °C, (b) the effects of GHSV on NO removal efficiency of MCAZ. (Reaction condition: (a) 1000 ppm NO, NH_3/NO: 1, 5% O_2, 500 mg of sample, 350 mL/min total flow rate and GHSV 20,000 h^{-1}; (b) 1000 ppm NO, NH_3/NO: 1, 5% O_2, 500 mg of sample, total flow rate 260 mL/min, 350 mL/min, 525 mL/min, 700 mL/min; GHSV 15,000 h^{-1}, 20,000 h^{-1}, 30,000 h^{-1}, 40,000 h^{-1}.)

Compared with other catalysts, MCAS gave a rather unpromising efficiency at low temperature. It is likely that the low activity of MCAS was rendered by the addition of SiO_2 and the decrease of Al_2O_3 content, which meant that the increase of activity was largely due to temperature rise rather than the synergism of the two oxides in the support. The curve of MCAT performance was much similar with that of MCA except that the latter showed a bit more active at middle-high temperature (180–320 °C). It could be conjectured that Ti did not play a mutual promotion role in the course of the SCR using MCAT (at least when the preparation method above was used). Additionally, it could be observed that MCAZ took the lead in all the temperature range compared with MCA. A broad high-efficiency temperature range was observed in low-middle-high temperature, that meant MCAZ could withstand the frequently variation of the temperature in the SCR.

3.1.2. The stability of the catalysts and the effect of GHSV

The results of reacting stability of MCA and MCAZ at 150 °C, 200 °C and 250 °C were shown in Fig. 3(a). With time went by, the efficiency of MCAZ and MCA showed almost no decline after 24 h. Actually, all the efficiencies decayed a little except for those of MCAZ at 200 °C and 250 °C. A contiguous tendency of decrease could be predicted because of the deposition of the ammonium nitrate or other by-products on the active sites at lower temperature. Nevertheless, MCAZ showed not only higher efficiency but also slighter decline in this set of tests. The capacity of MCAZ to process different flue gas load was measured by the GHSV tests (Fig. 3(b)). When the GHSV was 15,000 h^{-1}, higher NO removal efficiency was yielded across all the temperature range. On the whole, higher GHSV corresponded to lower activity, and GHSV showed a more apparent effect at low temperature (100–180 °C) than that at middle-high temperature (180–300 °C). It meant the reaction could sustain stable efficiency when the load of flue gas changed, namely, the fluctuation of processing load could hardly affect the performance of MCAZ at middle-high temperature. The fine stability of MCAZ was attributed to the porosity characteristics: as the entry and the exit of flue gas were more convenient due to the suitable pore size, the NO removal efficiency could stay at a high level for a long time.

3.1.3. The activity with H_2O and SO_2 in the system

Water vapor and SO_2 always play significant roles in NH_3-SCR because of their deactivation effects. Therefore a comparative study was conducted to measure the performance of MCA and

MCAZ in this regard. In Fig. 4 the solid and dot lines represented the SCR performance of MCAZ and MCA respectively.

Fig. 4(a) illustrated the comparison study on the SCR activity in the simulated flue gas with SO_2. When the temperature was 250 °C, both the MCA and MCAZ could obtain a normal efficiency at the beginning time. Afterward both efficiencies began to decline, but MCAZ was less influenced with a drop of 11% (94.7–83.4%). Meanwhile, the efficiency of MCA descended 22% (90.3–68.3%) and a continuous declining trend was observed as time went by. It indicated the participation of zirconium had certain effects on reducing the deactivation brought by SO_2. As shown in Fig. 4(b), the NO removal efficiency remained approximately 95% with 5% water vapor in system at 250 °C. However, when the reaction temperature was 150 °C, the results changed. The activity curve showed an obvious decay and a downward trend. Yet the deactivation was reversible after the H_2O (g) was purge out of the system at 150 °C. The curve remained almost horizontal in the reminding time (2.5 h) at 200 °C. It implied that H_2O vapor could hardly stay and deposit in the pores of MCAZ at 200 °C or higher temperature. Fig. 4(c) illustrated the activity performance of MCAZ and MCA in the system with SO_2 and water vapor simultaneously. The synergistic deactivating effect of the H_2O and SO_2 handicapped the performance of both catalysts greatly because they both faced a large decline after the addition of SO_2 and H_2O. Surprisingly, as a function of the zirconium loading, MCAZ owned much better performance than MCA at every temperature though the curve trends of them were similar. In addition, the results were in accord with other articles at the point that the deactivation of SO_2 is irreclaimable [24,35]. When the SO_2 stream was cut off, the efficiency could not return to the level before.

3.2. Characterization of catalysts

3.2.1. Specific surface area and pore diameter analysis

The BET specific surface area, BJH pore volume and pore diameter are summarized in Table 1.

The specific surface area of the samples decreased in the following order: MCAS > MCAZ > MCAT > MCA. MCAS owned the highest specific surface area since the particle of SiO_2 is finer than that of others. However, there have been articles reporting that catalysts containing SiO_2 as support or active component always give unsatisfactory performance due to its less active sites and inactive surface properties [36]. As can be seen in Table 1, catalysts with binary-oxides support possessed higher specific surface area than MCA, which revealed that the addition of TiO_2 and ZrO_2 into γ-Al_2O_3 could expand the specific surface area to a certain extent. Researchers who probed into the relationship between specific surface area and SCR activity elucidated that the material owning higher specific surface area always provided more reactive sites for the reactants [8], by which the reaction of NO conversion could be partially promoted. After the addition of ZrO_2, the specific surface area of MCAZ raised about 26%, so the higher specific surface area might be a reason for the superiority to MCA. Interestingly, compared with many other SCR catalysts [37–39], the pore diameters of the catalysts (40–86 nm) were rather big. It was inferred that the bigger size of the pore facilitated the entry, stay and collision for the reactants. Moreover, the catalysts with broader pore diameter could cope with high GHSV since it promoted the entrance and storage of the gas. Similarly, benefited from the broader pore, the catalysts would be difficult to get clogged and passivated, hence it was capable in the simulated flue gas with SO_2 and H_2O. However, it was unexpected that the pore volume diminished as the pore size got smaller. To explain this, the pore size distribution should be taken into consideration, as pore volume characteristic is determined by macropore and mesopore primarily, with ascopore and micropore as auxiliary.

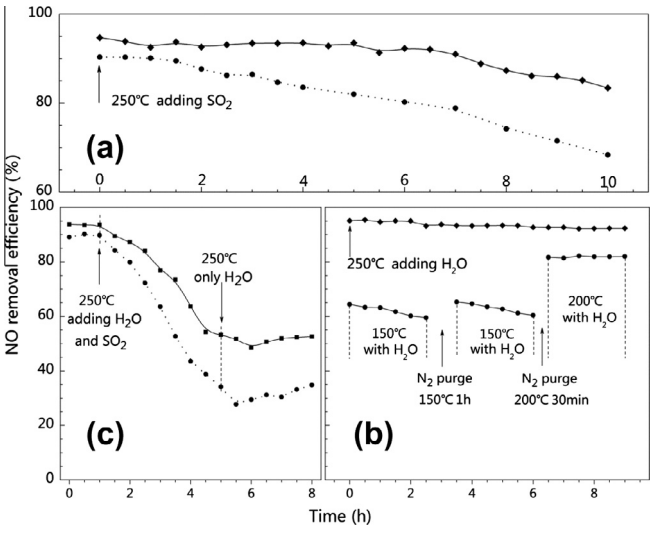

Fig. 4. NO removal efficiency of MCA and MCAZ in the flue gas consisting of (a) 1000 ppm NO, 1000 ppm NH_3, 5% O_2, 500 ppm SO_2 and N_2 as balance; (c) 1000 ppm NO, 1000 ppm NH_3, 5% O_2, 500 ppm SO_2, 5% H_2O vapor and N_2 as balance; (b) NO removal efficiency of MCAZ in the flue gas consisting of 1000 ppm NO, 1000 ppm NH_3, 5% O_2, 5% H_2O vapor and N_2 as balance.

3.2.2. XRD analysis of catalysts

The powder X-ray diffraction patterns of MCA, MCAS, MCAT and MCAZ are shown in Fig. 5.

Different oxides component in the supports were labeled: γ-Al_2O_3 (Tetragonal, PDF-#46-1131), ZrO_2 (Tetragonal, PDF-#79-1770), TiO_2 (Anatase, tetragonal, PDF-#75-1537) and MnO_2 (Tetragonal, PDF-#44-0141). For MCA, the crystal phases appeared at 2θ = 32.5°,36.76°, 45.64° and 66.98° were diffraction peaks of γ-Al_2O_3. The intensity of the peaks belonging to γ-Al_2O_3 decreased dramatically when a secondary metal oxide was added. Except for the major peak at 66.98°, other diffraction peaks of γ-Al_2O_3 were barely detected, while MCAT and MCAZ showed sharp characteristic peaks of themselves. The peaks of SiO_2 were hard to confirm due to the variety of possibilities of Si–Al–O. The characteristic peaks of MnO_2, Mn_2O_3, CeO_2 and Ce_2O_3 could be hardly detected in all four patterns, which was due to the widely dispersion and poorer crystalline on the surface. Be consistent with other literatures, MnO_x and CeO_y existed as highly dispersed amorphous states [26,37,40], which were beneficial for the reduction–oxidation in the SCR.

3.2.3. XPS study

The XPS spectra for Mn_{2p}, Ce_{3d}, O_{1s} levels of compounds from various catalysts are shown in Figs. 6–8. After a nonlinear background was subtracted, the peaks were deconvoluted into several sub-bands using the Gaussian function.

3.2.3.1. Mn. From Fig. 6, it can be seen that Mn 2p region contained a spin–orbit doublet with Mn $2p_{1/2}$ ranging a binding energies (BE) of 649.2–568.6 eV and Mn $2p_{3/2}$ ranging a BE of 637–649.2 eV. In consideration of the nitrate in the precursor, three types of photoelectron with different binding energies could be observed in all samples, which indicated that there were three species of Mn compounds. The peaks at 641.3 eV, 642,2 eV and 644.2–644.5 eV should be assigned to Mn_2O_3, MnO_2 and manganese nitrate respectively. This was in good agreement with several other literatures [41–44]. The manganese nitrate existed for the reason that the nitrate in the preparing system was not decomposed completely. Based on a series of thermodynamic calculations, the decomposition of

Table 1
The specific surface area, pore volume and pore diameter of the samples.

Catalysts	BET surface area (m^2/g)	Pore volume (cm^3/g)	Average pore diameter (nm)
MCA	129.09	0.3584	86.226
MCAS	180.94	0.1984	40.257
MCAT	141.72	0.299	60.063
MCAZ	163.51	0.2728	50.347

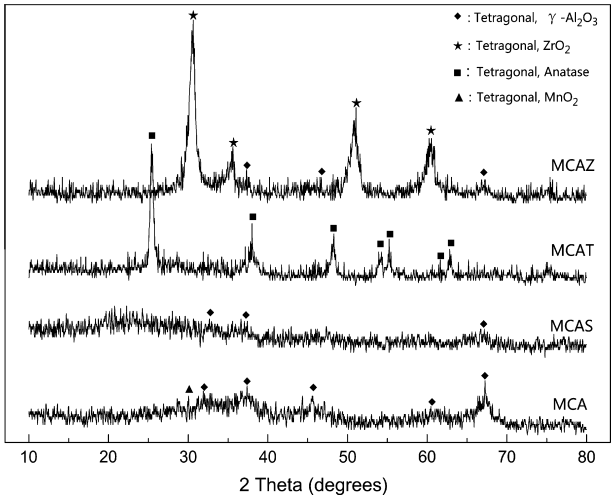

Fig. 5. XRD patterns of MCA, MCAZ, MCAT and MCAS.

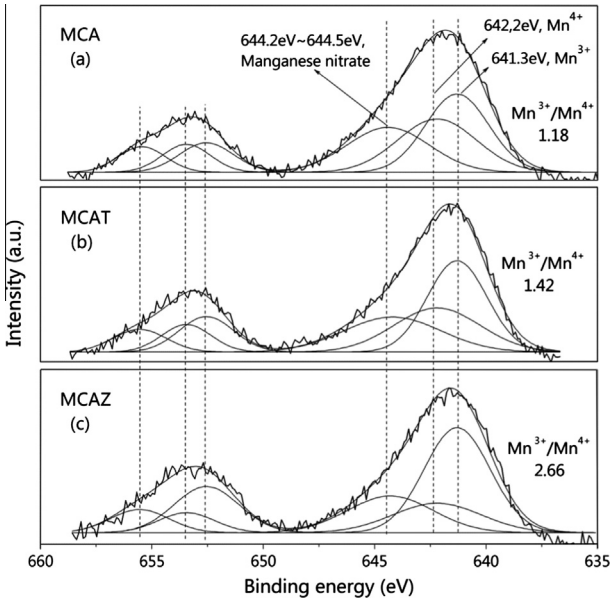

Fig. 6. Mn_{2p} XPS spectra for MCA, MCAT and MCAZ.

MnO_2 to Mn_2O_3 happened at 880 K and the decomposition of Mn_2O_3 to Mn_3O_4 happens at 1000–1200 K [45]. During the process of preparation, the samples were calcined at the temperature of 500 °C (773.15 K) for 4 h, so the manganese oxides existed at the states of MnO_2 and Mn_2O_3 in the samples. After the addition of ZrO_2, the ratio of Mn^{3+} and Mn^{4+} changed from 1.18 to 2.66, which is beneficial for the NO removal efficiency because the Mn_2O_3 was more activity in the reduction [44] due to the high dispersion and the low degrees of crystallinity in the catalyst. In addition, Lee et al. [4], Smirniotis et al. [41] and Thirupathi and Smirniotis [39]

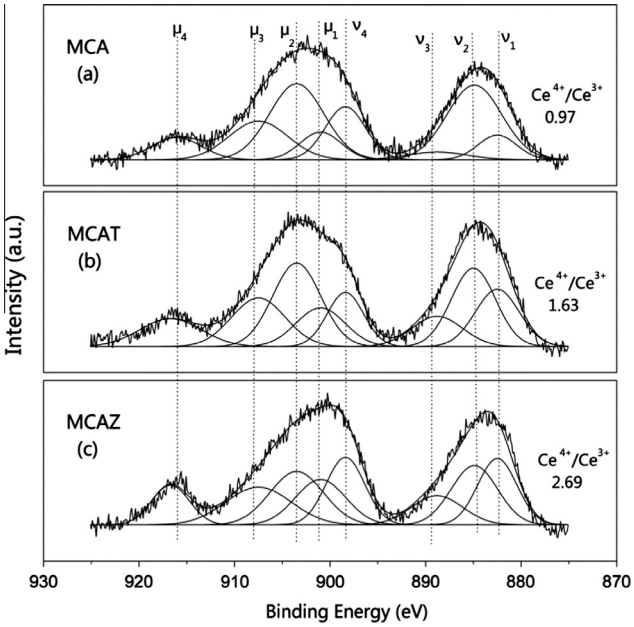

Fig. 7. Ce_{3d} XPS spectra for MCA, MCAT and MCAZ.

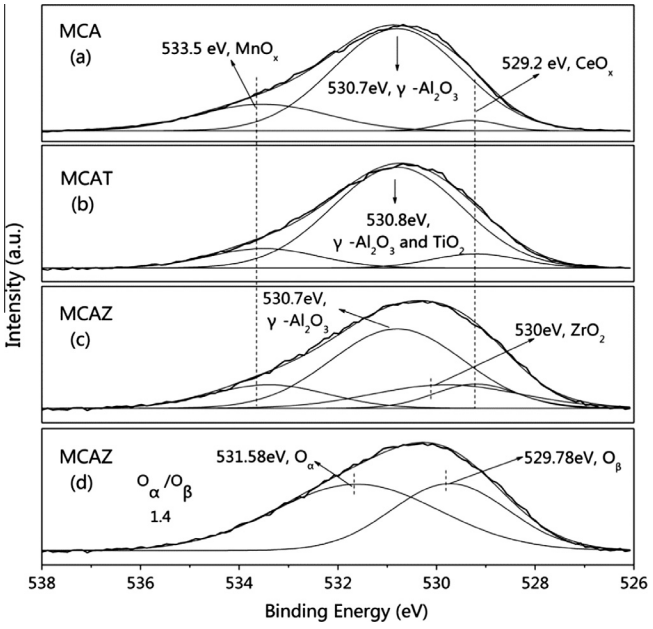

Fig. 8. O_{1s} XPS spectra for MCA, MCAT and MCAZ.

have pointed out that amorphous MnO_2 also bring a promotion of NO conversion because of its oxidation capacity. A small amount of amorphous MnO_2 existing on the surface of the samples was a subordinate reason for excellent SCR performance.

3.2.3.2. Ce. In Fig. 7, the peaks labeled ν were assigned to the Ce $3d_{5/2}$, and those labeled μ correspond to Ce $3d_{3/2}$. The spectra exhibited six features of Ce^{4+} (doublets ν_1/μ_1, ν_3/μ_3 and ν_4/μ_4) and two features of Ce^{3+} (doublets ν_2/μ_2) [8,26]. It is apparent that the Ce^{4+} and Ce^{3+} were coexisting but the ratio of them changed. The Ce^{4+}/Ce^{3+} improved from 0.97 to 1.63 and 2.69 after the addition of a secondary metal. Accordingly, on the surface of MCAT and MCAZ, Ce^{4+} was more dominate while Ce^{4+} and Ce^{3+} functioned

together to achieve high efficiency. The special redox couple Ce^{4+}/Ce^{3+}, in the form of CeO_2/Ce_2O_3, could easily generate labile oxygen vacancies and highly mobile oxygen during the process of the redox shift [8,46]. The reduced state specie Ce^{3+}, together with Mn^{3+}, played a role in creating charge imbalance, vacancies and unsaturated chemical bonds [26]. The function of oxidation state specie Ce^{4+} and Mn^{4+} was inferred to be assisting both the H-abstraction of NH_3 (to provide NH_2) and the formation of reactive nitrite intermediates at low temperature, together with O_2 adsorbed on the surface [47].

3.2.3.3. O. In Fig. 8, potential existence of each kind of O species was presented. The peaks appearing at binging energies value 533.5 eV, 529.2 eV, 530.7 eV and 530 eV could be attributed to the oxygen from MnO_x, CeO_y, γ-Al_2O_3 and ZrO_2, respectively [41,48–50]. In Fig. 8 (b), the peak at binding energy value 530.8 eV represented the oxygen in γ-Al_2O_3 and TiO_2 [51]. The ratio of the oxygen in active component and supports in each sample was calculated. The lowest value (0.24) appeared in MCAT, while the highest value (0.35) belonged to MCAZ, which meant that there was a slightly bigger amount of MnO_x and CeO_y on the surface of γ-Al_2O_3–ZrO_2 than on other supports.

From another point of view, the oxygen in the catalysts could be divided into two kinds of species: the lattice oxygen (529.78 eV, denoted as O_β) and the chemisorbed oxygen or/and weakly bonded oxygen species (531.58 eV, denoted as O_α) [8,52]. In the MCAZ, the O_α/O_β value came to 1.4 (Fig. 8(d)), that meant the chemisorbed oxygen was predominant on the surface of MCAZ. The chemisorbed oxygen was identified extensively as the most active oxygen which brings a great improvement in oxidation reaction [8,35,52].

3.2.4. H_2-TPR analysis

The reduction/oxidation (redox) properties of the catalysts were demonstrated by H_2-TPR (Fig. 9). The overlapping peaks in all profiles were deconvoluted using Gaussian function to several separate peaks corresponding to different species of MnO_x and CeO_y. As shown in Fig. 9, it was apparent that the redox abilities differed though same active component were used, namely, these differences were brought by the discrepancy of supports. Ettireddy et al. [53], Shen et al. [29] and Trawczyński et al. [54] demonstrated that MnO_x was reduced by H_2 in the following order: $MnO_2 \rightarrow Mn_2O_3 \rightarrow Mn_3O_4 \rightarrow MnO$. Therefore, the first low temperature peaks were correlated to reduction of MnO_2 while the peaks near 350 °C were attributed to reduction of Mn_2O_3, this favored well with the papers aforementioned. After doping TiO_2 and ZrO_2 in the support, the reduction temperature of MnO_2 shifted to lower position, which reflected the increase of oxygen mobility within the low temperature range. Among these profiles, the peak of MnO_2 in MCAZ shifted about 44 °C to lower temperature and this could contribute to the better low temperature activity of MCAZ in comparison with that of the other two catalysts. Besides, the peaks at 595 °C, 581 °C and 566 °C were attributed to the reduction of CeO_2 [29]; it could be seen that the interaction of the two metal oxides in the supports shifted the reduction peak of CeO_2 to lower temperature as well. Furthermore, the area ratios of the first reduction peaks to the second ones for MCA, MCAT and MCAZ were 0.87, 0.42 and 0.37, respectively. These indicated that the dominant MnO_x species in MCAZ appeared to be Mn_2O_3, which was in fine consistence with the XPS results though the specific ratio figures were not the same. Considering the higher catalytic activity of MCAZ at low temperature and the XRD results together, it might be reasonable to speculate that highly dispersed amorphous Mn_2O_3 was more favorable for NO catalytic oxidation than MnO_2. Literatures also reported that the weaker Mn^{3+}–O bond favored the catalytic oxidation of NO due to its lower strength, and this promoted the generation and release of NO_2 produced as well [55,56].

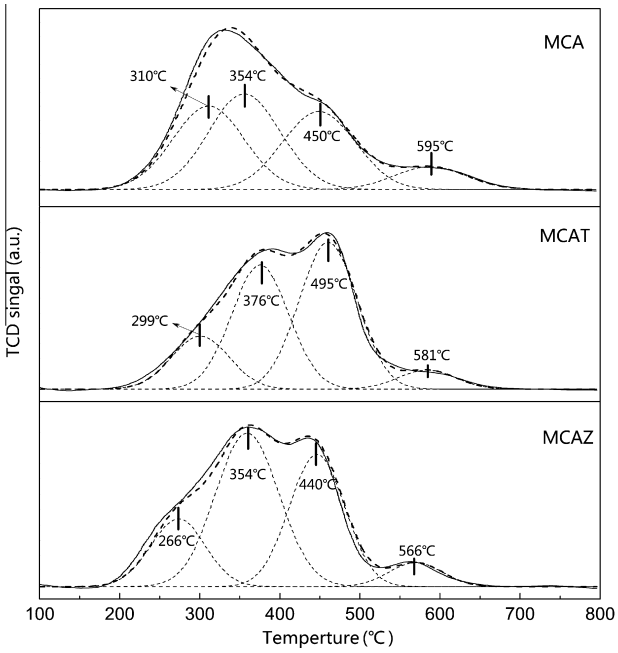

Fig. 9. Deconvoluted H_2-TPR profiles of MCA, MCAT and MCAZ.

3.2.5. FTIR study

The FTIR spectra of pre-prepared samples of MCAZ were analyzed with peak deconvolution.

3.2.5.1. NH_3 and NO + O_2 FTIR. The NH_3 and (NO + O_2) FTIR spectra of MCAZ was shown in Fig. 10(a). The strongest band at 1611 cm^{-1} should be associated with the asymmetric deformation vibration of NH_3 ($\delta_{as}(NH_3)$) which was adsorbed on Lewis acid sites [57]. There were no remarkable bands at the regions belonging to Brønsted acid sites [57,58]. Other N–H vibrations were weaker but dispersed widely, the wavenumbers were as follows: 1530 cm^{-1} ($\delta_s(NH_3)$ of the $-NH_3^+$ group decomposed from $-NH_4^+$ [57,59]), 1489 cm^{-1} ($\delta_{as}(NH_4^+)$ on Mn sites and Al_2O_3 sites [41] and/or the δ(N–H) from the amines or amides [18]), 1402 cm^{-1} and 1262 cm^{-1} (coordinate NH_3 species [41]). The weak band at 1356 cm^{-1} was conjectured as the oxidized species such as nitrate or nitrite because MnO_x–CeO_y is highly active for oxidation of ammonia at low temperatures [18]. The spectra clearly demonstrated the interaction of NH_3 with MCAZ in these different ways: coordination on Lewis acid sites, protonation and deprotonation of ammonia, formation of amid species, being oxidized by active oxygen. It also could be seen that most NH_3 was adsorbed and coordinated on the Lewis acid sites because of the acidic property of the material. In (NO + O_2) FTIR curve, the adsorbed N species existed mainly as nitrate because the strongest band was assigned to bridging bidentate nitrate species (ν(N=O), 1624 cm^{-1}) [60,61]. Zhang et al. [62] demonstrated that among monodentate, isolated, bidentate and bridging nitrates adsorbed on the Al_2O_3, the last two owned the weakest thermal stability, which meant that the adsorbed nitrates could participate in the redox reaction sufficiently. Two overlapping bands, located at 1548 cm^{-1} (bridging nitrate species and/or N_2O_3 [63]) and 1502 cm^{-1} (monodentate nitrate), were much smaller. The formation of the band in the 1280–1480 cm^{-1} could be attributed in part to the reaction of produced NO_2 with surface oxygen. The band could be deconvoluted to three bands at 1354 cm^{-1} (nitrito), 1380 cm^{-1} (NO_2 stretch in NO_3^-) and 1410 cm^{-1} (monodentate nitrate) [61,64]. Besides, two weak bands at 1768 cm^{-1} and 1267 cm^{-1} could be assigned to adsorbed

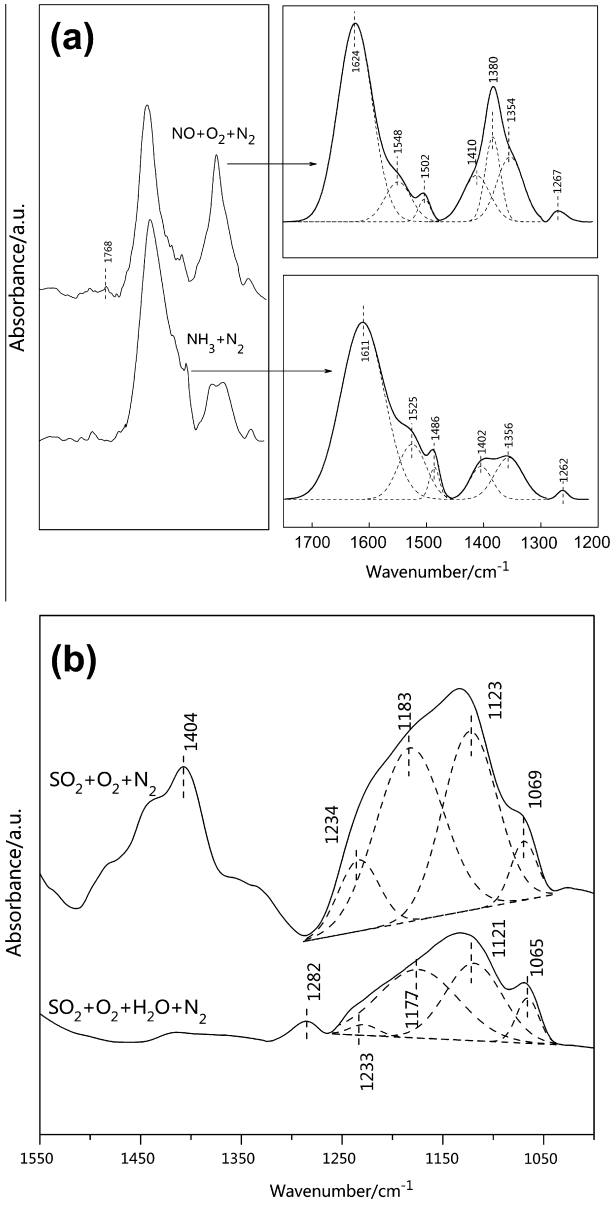

Fig. 10. Deconvoluted FTIR spectra for MCAZ purged by (a) NH_3 and ($NO + O_2$), (b) ($SO_2 + O_2$) and ($SO_2 + O_2 + H_2O$).

N_2O_4 derived from NO_2 at low temperature [60,63] and chelating nitro [60,61], respectively.

In fact, the mechanism of NH_3-SCR on MnO_x has been investigated using in situ FTIR coupled with transient isotopic labeled studies [65]. The literature reported that the lattice oxygen on the surface of catalyst acted as a "transfer station" in the NH_3-SCR, especially in the oxidation of NH_3, while the main job of the gaseous oxygen in the flue gas was filling the vacancies over the catalyst surface. The reaction between adsorbed (or coordinated) ammonia and lattice oxygen was practically instantaneous, and the NO participated in the process by forming nitrites and exchanging oxygen with the lattice oxygen on the surface. The N from the NH_3 and the N from the NO stayed on the catalyst for a long time and underwent some transitions between several active intermediates. After a series rearrangement of chemical bonds H_2O and N_2 were generated as products. Afterward the gaseous oxygen filled the vacancies again before the beginning of next reduction–oxidation cycle. The discussion of FTIR above showed a brief description of NH_3 and NO adsorption. In connection with the results of H_2-TPR and XPS analysis of O (Section 3.2.3.3), it might be reasonable to speculate that the oxygen on the surface of the material not only supplied abundant chemisorbed and lattice oxygen, but also enhanced the oxidation of NH_3 and the formation of highly reactive surface nitrates. The nitrates possessed higher activity in the redox reaction with adsorbed NH_3 species comparing with NO_x, which promoted the NO removal efficiency as well.

3.2.5.2. $SO_2 + O_2$ FTIR. The $SO_2 + O_2$ and $SO_2 + H_2O + O_2$ FTIR spectra of MCAZ were shown in Fig. 10(b). The curve of $SO_2 + O_2$ FTIR showed a band at 1404 cm^{-1}, that evidenced the adsorbed gaseous SO_2 deposited on the surface of the catalysts [66]. The other curve did not have this band since the SO_2 reacted with H_2O and O_2 to form sulfite and/or sulfate. Goodman et al. [67] and Mitchel et al. [68] investigated SO_2 adsorption on γ-Al_2O_3 particles and found that the band centered at 1065 cm^{-1} was assigned to adsorbed SO_2 identified as sulfite, more specially, the band could be assigned to ν_s(S=O) of HSO_3^- (1100–1000 cm^{-1}), referenced from *the Sadtler handbook of infrared spectra* [69]. In addition, the band at 1234 cm^{-1} and 1233 cm^{-1} could be attributed to ν_{as}(S=O) of HSO_3^- in sulfonic acids [69]. Peak et al. [70] reported that the band between 1250 and 1050 cm^{-1} was the mainly infrared sulfate vibrations that were accessible to FTIR investigation. Two possible bidentate sulfates might exist: bidentate binuclear sulfate and bidentate mononuclear sulfate. The existence of the later would shift the band to higher wavenumbers (much higher than was observed); thus the bands at 1123 cm^{-1} were assigned to asymmetric stretching bands of bidentate binuclear sulfate. The bands around 1170 cm^{-1} were uncertain since the bidentate SO_4^{2-} could bridge with metallic cations, proton and/or hydrogen bond. Chang et al. [58,71] held the opinion that the bidentate sulfate could provide new acid sites for NH_3 adsorption and the emerging sites were mainly Lewis acid sites, as characterized by pyridine IR. The poison mechanism of SO_2 is widely discussed and a common opinion is that the existence of SO_2 in the system promotes the formation of $M(SO_4)_x$, in which M represents NH_4^+, Mn, Ce, Al, or some cations taking part in the SCR [40]. However, the sulfates and sulfites play a role in proliferating acidity, especially the Lewis acid sites on the surface, benefit from which NH_3 adsorption is enhanced and the formation of the intermediate $-NH_3^+$ is promoted [57], thus the SCR activity of MCAZ was better than MCA in the flue gas with SO_2 (shown in Fig. 4). It is noteworthy that the adsorbed SO_2 could inhibit neither the depositions of $(NH_4)_2SO_4/NH_4HSO_4$ nor the competitive adsorption between SO_2 with NO on the Mn and Ce sites, namely, the promotion for NH_3 adsorption and the deactivation of SO_2 happened simultaneously. Therefore, the application of the catalyst in a flue gas with high concentration of SO_2 is probably challenging.

4. Conclusions

The modifying influence of TiO_2, SiO_2 and ZrO_2 were explored and analyzed in detail. When the mole ratio of Al_2O_3 to ZrO_2 was 3:1, MCAZ exhibited remarkable NO removal efficiency as well as slighter deactivation of SO_2 and H_2O in SCR. TiO_2 and SiO_2 in the support prepared by given synthetic methods seems no significant improvement to the catalysts' performance. It was confirmed that the addition of secondary metal could improve the specific surface area of MnO_x–CeO_2/Al_2O_3. After doping with ZrO_2, the crystallinity and the valence of the surface elements have been changed for the promoting of the reaction: more amorphous states Mn_2O_3 and coexisting Ce^{3+}/Ce^{4+} led to the perfect performance in the low temperature. More efficient redox ability was also obtained after the doping of ZrO_2. In addition, the surface acidity, adsorbed nitrates

and adsorbed bidentate sulfates were inferred to be propitious to excellent performance by FTIR.

Acknowledgements

The project is financially supported by the National Natural Science Foundation of China (51278177), the National High Technology Research and Development Program of China (863 Program, No. 2011AA060803) and the Scientific and Technological Major Special Project of Hunan Province in China (2010XK6003).

Appendix A. Supplementary material

Supplementary data associated with this article can be found, in the online version, at http://dx.doi.org/10.1016/j.cej.2013.12.076.

References

[1] G. Busca, L. Lietti, G. Ramis, F. Berti, Chemical and mechanistic aspects of the selective catalytic reduction of NO_x by ammonia over oxide catalysts: a review, Appl. Catal. B: Environ. 18 (1998) 1–36.
[2] H. Bosh, F.J. Janssen, Formation and control of nitrogen oxides, Catal. Today 2 (1988) 369–379.
[3] S. Roy, M.S. Hegde, G. Madras, Catalysis for NO_x abatement, Appl. Energy 86 (2009) 2283–2297.
[4] S.M. Lee, K.H. Park, S.C. Hong, MnO_x/CeO_2–TiO_2 mixed oxide catalysts for the selective catalytic reduction of NO with NH_3 at low temperature, Chem. Eng. J. 195 (2012) 323–331.
[5] J.H. Ko, S.H. Park, J.K. Jeon, S.S. Kim, S.C. Kim, J.M. Kim, D. Chang, Y.K. Park, Low temperature selective catalytic reduction of NO with NH_3 over Mn supported on $Ce_{0.65}Zr_{0.35}O_2$ prepared by supercritical method: effect of Mn precursors on NO reduction, Catal. Today 185 (2012) 290–295.
[6] J. Li, H. Chang, L. Ma, J. Hao, R.T. Yang, Low-temperature selective catalytic reduction of NO_x with NH_3 over metal oxide and zeolite catalysts – a review, Catal. Today 175 (2011) 147–156.
[7] T.S. Park, S.K. Jeong, S.H. Hong, S.C. Hong, Selective catalytic reduction of nitrogen oxides with NH_3 over natural manganese ore at low temperature, Ind. Eng. Chem. Res. 40 (2001) 4491–4495.
[8] Z. Wu, R. Jin, Y. Liu, H. Wang, Ceria modified MnO_x/TiO_2 as a superior catalyst for NO reduction with NH_3 at low-temperature, Catal. Commun. 9 (2008) 2217–2220.
[9] Y. Huang, Z. Tong, B. Wu, J. Zhang, Low temperature selective catalytic reduction of NO by ammonia over V_2O_5–CeO_2/TiO_2, J. Fuel Chem. Technol. 36 (2008) 616–620.
[10] W.S. Kijlstra, J.C.M.L. Daamen, J.M. van de Graaf, B. van der Linden, E.K. Poels, A. Bliek, Inhibiting and deactivating effects of water on the selective catalytic reduction of nitric oxide with ammonia over MnO_x/Al_2O_3, Appl. Catal. B: Environ. 7 (1996) 337–357.
[11] T. Boningari, R. Koirala, P.G. Smirniotis, Low-temperature selective catalytic reduction of NO with NH_3 over V/ZrO_2 prepared by flame-assisted spray pyrolysis: Structural and catalytic properties, Appl. Catal. B: Environ. 127 (2012) 255–264.
[12] T. Boningari, R. Koirala, P.G. Smirniotis, Low-temperature catalytic reduction of NO by NH_3 over vanadia-based nanoparticles prepared by flame-assisted spray pyrolysis: influence of various supports, Appl. Catal. B: Environ. 140–141 (2013) 289–298.
[13] A. Sultana, M. Sasaki, H. Hamada, Influence of support on the activity of Mn supported catalysts for SCR of NO with ammonia, Catal. Today 185 (2012) 284–289.
[14] G. Qi, R.T. Yang, Performance and kinetics study for low-temperature SCR of NO with NH_3 over MnO_x–CeO_2 catalyst, J. Catal. 217 (2003) 434–441.
[15] R.Q. Long, R.T. Yang, The promoting role of rare earth oxides on Fe-exchanged TiO_2-pillared clay for selective catalytic reduction of nitric oxide by ammonia, Appl. Catal. B: Environ. 27 (2000) 87–95.
[16] F. Eigenmann, M. Maciejewski, A. Baiker, Selective reduction of NO by NH_3 over manganese-cerium mixed oxides: relation between adsorption, redox and catalytic behavior, Appl. Catal. B: Environ. 62 (2006) 311–318.
[17] G. Qi, R.T. Yang, R. Chang, MnO_x–CeO_2 mixed oxides prepared by co-precipitation for selective catalytic reduction of NO with NH_3 at low temperatures, Appl. Catal. B: Environ. 51 (2004) 93–106.
[18] G. Qi, R.T. Yang, Characterization and FTIR studies of MnO_x–CeO_2 catalyst for low-temperature selective catalytic reduction of NO with NH_3, J. Phys. Chem. B 108 (2004) 15738–15747.
[19] Z. Sheng, Y. Hu, J. Xue, X. Wang, W. Liao, SO_2 poisoning and regeneration of Mn–Ce/TiO_2 catalyst for low temperature NO_x reduction with NH_3, J. Rare Earth 30 (2012) 676–682.
[20] R. Jin, Y. Liu, Z. Wu, H. Wang, T. Gu, Low-temperature selective catalytic reduction of NO with NH_3 over Mn–Ce oxides supported on TiO_2 and Al_2O_3: a comparative study, Chemosphere 78 (2010) 1160–1166.
[21] R. Jin, Y. Liu, Z. Wu, H. Wang, T. Gu, Relationship between SO_2 poisoning effects and reaction temperature for selective catalytic reduction of NO over Mn–Ce/TiO_2 catalyst, Catal. Today 153 (2010) 84–89.
[22] G. Carja, Y. Kameshima, K. Okada, C.D. Madhusoodana, Mn–Ce/ZSM5 as a new superior catalyst for NO reduction with NH_3, Appl. Catal. B: Environ. 73 (2007) 60–64.
[23] Z. Liu, P.J. Millington, J.E. Bailie, R.R. Rajaram, J.A. Anderson, A comparative study of the role of the support on the behaviour of iron based ammonia SCR catalysts, Micropor. Mesopor. Mater. 104 (2007) 159–170.
[24] G. Xie, Z. Liu, Z. Zhu, Q. Liu, J. Ge, Z. Huang, Simultaneous removal of SO_2 and NO_x from flue gas using a CuO/Al_2O_3 catalyst sorbent I. Deactivation of SCR activity by SO_2 at low temperatures, J. Catal. 224 (2004) 36–41.
[25] B.M. Reddy, P. Lakshmanan, A. Khan, Investigation of surface structures of dispersed V_2O_5 on CeO_2–SiO_2, CeO_2–TiO_2, and CeO_2–ZrO_2 mixed oxides by XRD, Raman, and XPS techniques, J. Phys. Chem. B 108 (2004) 16855–16863.
[26] C. Liu, L. Chen, J. Li, L. Ma, H. Arandiyan, Y. Du, J. Xu, J. Hao, Enhancement of activity and sulfur resistance of CeO_2 supported on TiO_2–SiO_2 for the selective catalytic reduction of NO by NH_3, Environ. Sci. Technol. 46 (2012) 6182–6189.
[27] B.M. Reddy, I. Ganesh, B. Chowdhury, Design of stable and reactive vanadium oxide catalysts supported on binary oxides, Catal. Today 49 (1999) 115–121.
[28] M. Ouzzine, G.A. Cifredo, J.M. Gatica, S. Harti, T. Chafik, H. Vidal, Original carbon-based honeycomb monoliths as support of Cu or Mn catalysts for low-temperature SCR of NO: effects of preparation variables, Appl. Catal. A: Gen. 342 (2008) 150–158.
[29] B. Shen, Y. Wang, F. Wang, T. Liu, The effect of Ce–Zr on NH_3–SCR activity over $MnO_{x(0.6)}/Ce_{0.5}Zr_{0.5}O_2$ at low temperature, Chem. Eng. J. 236 (2014) 171–180.
[30] N. Jagtap, S.B. Umbarkar, P. Miquel, P. Granger, M.K. Dongare, Support modification to improve the sulphur tolerance of Ag/Al_2O_3 for SCR of NO_x with propene under lean-burn conditions, Appl. Catal. B: Environ. 90 (2009) 416–425.
[31] S.M. Park, H. Jang, E.S. Kim, H. Han, G. Seo, Incorporation of zirconia onto silica for improved Pt/SiO_2 catalysts for the selective reduction of NO by H_2, Appl. Catal. A: Gen. 427–428 (2012) 155–164.
[32] A. Sultana, M. Haneda, T. Fujitani, H. Hamada, Influence of Al_2O_3 support on the activity of Ag/Al_2O_3 catalysts for SCR of NO with decane, Catal. Lett. 114 (2007) 96–102.
[33] M. Stanciulescu, G. Caravaggio, A. Dobri, J. Moir, R. Burich, J.P. Charland, P. Bulsink, Low-temperature selective catalytic reduction of NO_x with NH_3 over Mn-containing catalysts, Appl. Catal. B: Environ. 123 (2012) 229–240.
[34] A. Shi, X. Wang, T. Yu, M. Shen, The effect of zirconia additive on the activity and structure stability of V_2O_5/WO_3–TiO_2 ammonia SCR catalysts, Appl. Catal. B: Environ. 106 (2011) 359–369.
[35] B. Shen, Y. Yao, H. Ma, T. Liu, Ceria modified MnO_x/TiO_2-pillared clays catalysts for the selective catalytic reduction of NO with NH_3 at low temperature, Chinese J. Catal. 32 (2011) 1803–1811.
[36] H. Xu, Y. Shen, C. Shao, F. Lin, S. Zhu, T. Qiu, A novel catalyst of silicon cerium complex oxides for selective catalytic reduction of NO by NH_3, J. Rare Earth 28 (2010) 721–726.
[37] W. Zhao, C. Li, P. Lu, Q. Wen, Y. Zhao, X. Zhang, C. Fan, S. Tao, Iron, lanthanum and manganese oxides loaded on γ-Al_2O_3 for selective catalytic reduction of NO with NH_3 at low temperature, Environ. Technol. 34 (2013) 81–90.
[38] H. Xu, Q. Zhang, C. Qiu, T. Lin, M. Gong, Y. Chen, Tungsten modified MnO_x–CeO_2/ZrO_2 monolith catalysts for selective catalytic reduction of NO_x with ammonia, Chem. Eng. Sci. 76 (2012) 120–128.
[39] B. Thirupathi, P.G. Smirniotis, Co-doping a metal (Cr, Fe Co, Ni, Cu, Zn, Ce, and Zr) on Mn/TiO_2 catalyst and its effect on the selective reduction of NO with NH_3 at low-temperatures, Appl. Catal. B: Environ. 110 (2011) 195–206.
[40] Z. Wu, R. Jin, H. Wang, Y. Liu, Effect of ceria doping on SO_2 resistance of Mn/TiO_2 for selective catalytic reduction of NO with NH_3 at low temperature, Catal. Commun. 10 (2009) 935–939.
[41] P.G. Smirniotis, P.M. Sreekanth, D.A. Pena, R.G. Jenkins, Manganese oxide catalysts supported on TiO_2, Al_2O_3, and SiO_2: a comparison for low-temperature SCR of NO with NH_3, Ind. Eng. Chem. Res. 45 (2006) 6436–6443.
[42] B. Thirupathi, P.G. Smirniotis, Nickel-doped Mn/TiO_2 as an efficient catalyst for the low-temperature SCR of NO with NH_3: catalytic evaluation and characterizations, J. Catal. 288 (2012) 74–83.
[43] D.A. Peña, B.S. Uphade, P.G. Smirniotis, TiO_2-supported metal oxide catalysts for low-temperature selective catalytic reduction of NO with NH_3 I. Evaluation and characterization of first row transition metals, J. Catal. 221 (2004) 421–431.
[44] J. Li, J. Chen, R. Ke, C. Luo, J. Hao, Effects of precursors on the surface Mn species and the activities for NO reduction over MnO_x/TiO_2 catalysts, Catal. Commun. 8 (2007) 1896–1900.
[45] J. Xie, D. Fang, F. He, J. Chen, Z. Fu, X. Chen, Performance and mechanism about MnO_x species included in MnO_x/TiO_2 catalysts for SCR at low temperature, Catal. Commun. 28 (2012) 77–81.
[46] B.M. Reddy, A. Khan, Y. Yamada, T. Kobayashi, S. Loridant, J.C. Volta, Structural characterization of CeO_2–TiO_2 and V_2O_5/CeO_2–TiO_2 catalysts by Raman and XPS techniques, J. Phys. Chem. B 107 (2003) 5162–5167.
[47] W.S. Kijlstra, D.S. Brands, H.I. Smit, E.K. Poels, A. Bliek, Mechanism of the selective catalytic reduction of NO with NH_3 over MnO_x/Al_2O_3, J. Catal. 171 (1997) 219–230.
[48] A. Galtayries, R. Sporken, J. Riga, G. Blanchard, R. Caudano, XPS comparative study of ceria/zirconia mixed oxides: powders and thin film characterisation, J. Electron. Spectrosc. 88–91 (1998) 951–956.

[49] T.L. Barr, An ESCA study of the termination of the passivation of elemental metals, J. Phys. Chem. 82 (1978) 1801–1810.
[50] T.L. Barr, The nature of the relative bonding chemistry in zeolites: an XPS study, Zeolites 10 (1990) 760–765.
[51] D. Leinen, A. Fernández, J.P. Espinós, J.P. Holgado, A.R. González-Elipe, An XPS study of the mixing effects induced by ion bombardment in composite oxides, Appl. Surf. Sci. 68 (1993) 453–459.
[52] H. Li, C. Wu, Y. Li, J. Zhang, CeO_2–TiO_2 catalysts for catalytic oxidation of elemental mercury in low-rank coal combustion flue gas, Environ. Sci. Technol. 45 (2011) 7394–7400.
[53] P.R. Ettireddy, N. Ettireddy, S. Mamedov, P. Boolchand, P.G. Smirniotis, Surface characterization studies of TiO_2 supported manganese oxide catalysts for low temperature SCR of NO with NH_3, Appl. Catal. B: Environ. 76 (2007) 123–134.
[54] J. Trawczyński, B. Bielak, W. Miśta, Oxidation of ethanol over supported manganese catalysts-effect of the carrier, Appl. Catal. B: Environ. 55 (2005) 277–285.
[55] I. Atribak, A. Bueno-López, A. García-García, P. Navarro, D. Frías, M. Montes, Catalytic activity for soot combustion of birnessite and cryptomelane, Appl. Catal. B: Environ. 93 (2010) 267–273.
[56] Z. Wu, N. Tang, L. Xiao, Y. Liu, H. Wang, MnO_x/TiO_2 composite nanoxides synthesized by deposition-precipitation method as a superior catalyst for NO oxidation, J. Colloid Interf. Sci. 352 (2010) 143–148.
[57] C. Zhou, Y. Zhang, X. Wang, H. Xu, K. Sun, K. Shen, Influence of the addition of transition metals (Cr, Zr, Mo) on the properties of MnO_x–FeO_x catalysts for low-temperature selective catalytic reduction of NO_x by ammonia, J. Colloid Interf. Sci. 392 (2013) 319–324.
[58] H. Chang, J. Li, X. Chen, L. Ma, S. Yang, J.W. Schwank, J. Hao, Effect of Sn on MnO_x–CeO_2 catalyst for SCR of NO_x by ammonia: enhancement of activity and remarkable resistance to SO_2, Catal. Commun. 27 (2012) 54–57.
[59] J.G. Amores, V.S. Escribano, G. Ramis, G. Busca, An FT-IR study of ammonia adsorption and oxidation over anatase-supported metal oxides, Appl. Catal. B: Environ. 13 (1997) 45–58.
[60] Q. Yu, X. Yao, H. Zhang, F. Gao, L. Dong, Effect of ZrO_2 addition method on the activity of Al_2O_3-supported CuO for NO reduction with CO: impregnation vs. coprecipitation, Appl. Catal. A: Gen. 423 (2012) 42–51.
[61] Y. Chi, S.S.C. Chuang, Infrared study of NO adsorption and reduction with C_3H_6 in the presence of O_2 over CuO/Al_2O_3, J. Catal. 190 (2000) 75–91.
[62] X. Zhang, H. He, H. Gao, Y. Yu, Experimental and theoretical studies of surface nitrate species on Ag/Al_2O_3 using DRIFTS and DFT, Spectrochim. Acta A 71 (2008) 1446–1451.
[63] T. Weingand, S. Kuba, K. Hadjiivanov, H. Knozinger, Nature and reactivity of the surface species formed after NO adsorption and NO + O_2 coadsorption on a WO_3–ZrO_2 catalyst, J. Catal. 209 (2002) 539–546.
[64] Y. Chi, S.S.C. Chuang, The effect of oxygen concentration on the reduction of NO with propylene over CuO/γ-Al_2O_3, Catal. Today 62 (2000) 303–318.
[65] P.R. Ettireddy, N. Ettireddy, T. Boningari, R. Pardemann, P.G. Smirniotis, Investigation of the selective catalytic reduction of nitric oxide with ammonia over Mn/TiO_2 catalysts through transient isotopic labeling and in situ FT-IR studies, J. Catal. 292 (2012) 53–63.
[66] H. Cheng, Q. Liu, M. Huang, S. Zhang, R.L. Frost, Application of TG-FTIR to study SO_2 evolved during the thermal decomposition of coal-derived pyrite, Thermochim. Acta 555 (2013) 1–6.
[67] A.L. Goodman, P. Li, C.R. Usher, V.H. Grassian, Heterogeneous uptake of sulfur dioxide on aluminum and magnesium oxide particles, J. Phys. Chem. A 105 (2001) 6109–6120.
[68] M.B. Mitchell, V.N. Sheinker, M.G. White, Adsorption and reaction of sulfur dioxide on alumina and sodium-impregnated alumina, J. Phys. Chem. 100 (1996) 7550–7557.
[69] W.W. Simons, S.R. Laboratations, Sadtler Handbook of Infrared Spectra, Sadtler Research Laboratories, Philadelphia, 1978.
[70] D. Peak, R.G. Ford, D.L. Sparks, An in situ ATR-FTIR investigation of sulfate bonding mechanisms on goethite, J. Colloid Interf. Sci. 218 (1999) 289–299.
[71] H. Chang, X. Chen, J. Li, L. Ma, C. Wang, C. Liu, J.W. Schwank, J. Hao, Improvement of activity and SO_2 tolerance of Sn-modified MnO_x–CeO_2 catalysts for NH_3–SCR at low temperatures, Environ. Sci. Technol. 47 (2013) 5294–5301.